International Conference on Mathematics and Computational Methods Applied to Nuclear Science and Engineering (M&C 2011)
Rio de Janeiro, RJ, Brazil, May 8-12, 2011, on CD-ROM, Latin American Section (LAS) / American Nuclear Society (ANS)
ISBN 978-85-63688-00-2

MULTIGROUP AND COUPLED FORWARD-ADJOINT MONTE CARLO CALCULATION EFFICIENCIES FOR SECONDARY NEUTRON DOSES FROM PROTON BEAMS

Charles T. Kelsey IV[1,2] and Anil K. Prinja[1]
[1]Department of Chemical and Nuclear Engineering
MSC01 1120, 1 University of New Mexico, Albuquerque, NM 87131
kelsey@unm.edu; prinja@unm.edu

[2]Los Alamos Neutron Science Center
Los Alamos National Laboratory, P.O. Box 1663, M.S. H805, Los Alamos, NM 87545
ckelsey@lanl.gov

ABSTRACT

We evaluate the Monte Carlo calculation efficiency for multigroup transport relative to continuous energy transport using the MCNPX code system to evaluate secondary neutron doses from a proton beam. We consider both fully forward simulation and application of a midway forward-adjoint coupling method to the problem. Previously we developed tools for building coupled multigroup proton/neutron cross section libraries and showed consistent results for continuous energy and multigroup proton/neutron transport calculations. We observed that forward multigroup transport could be more efficient than continuous energy. Here we quantify solution efficiency differences for a secondary radiation dose problem characteristic of proton beam therapy problems. We begin by comparing figures of merit for forward multigroup and continuous energy MCNPX transport and find that multigroup is 30 times more efficient. Next we evaluate efficiency gains for coupling out-of-beam adjoint solutions with forward in-beam solutions. We use a variation of a midway forward-adjoint coupling method developed by others for neutral particle transport. Our implementation makes use of the surface source feature in MCNPX and we use spherical harmonic expansions for coupling in angle rather than solid angle binning. The adjoint out-of-beam transport for organs of concern in a phantom or patient can be coupled with numerous forward, continuous energy or multigroup, in-beam perturbations of a therapy beam line configuration. Out-of-beam dose solutions are provided without repeating out-of-beam transport.

Key Words: multigroup, Monte Carlo, forward-adjoint coupling, neutron dose, proton therapy

1. INTRODUCTION

Secondary neutrons produced by proton therapy beams result in second cancer risks that should be assessed and ideally minimized [1]. Doses from secondary neutrons are not always calculated during treatment planning due to difficulty and expense [2]. The radiation transport code MCNPX is one that is often used for these calculations and that has been extensively benchmarked for proton therapy applications [3,4]. Typically MCNPX is run in the forward mode using continuous energy cross section data. In previous work we observed that forward calculation efficiency could be higher using coupled multigroup proton/neutron cross section

data [5]. Here we investigate this further by comparing efficiency of continuous energy and multigroup forward calculation results obtained in the absence of other variance reduction techniques. We also investigate the efficiency of midway forward-adjoint coupling that permits forward continuous energy treatment for the in-beam portion of the problem while adjoint multigroup treatment is used for the out-of-beam portion of the problem. The motivation for this work is that more efficient methods may lead to more complete dose assessments during treatment planning.

We previously developed tools for building coupled multigroup proton/neutron cross section libraries from evaluated nuclear data and MCNPX physics models where evaluated data is unavailable [6]. We presented further library developments and consistency between multigroup and continuous energy Monte Carlo solutions in Ref. 5. For the present work we are using the multigroup data library described in Ref. 5. It is an 89-proton, 107-neutron group library for energies up to 400 MeV with 40 equiprobable cosine bins for scattering cross sections. This angular resolution was shown to be necessary for accurate secondary neutron dose solutions about proton beams incident on water. The cross sections are modified by a downscatter only energy straggling model and momentum transfer coefficients are included. The library also has energy deposition cross sections for the estimation of absorbed doses.

We use the figure of merit (FOM) reported for MCNPX tallies as a measure for comparing multigroup and continuous energy calculation efficiencies. For MCNPX the definition of FOM for a tally is

$$\mathrm{FOM} \equiv \frac{1}{\mathrm{FSD}^2 T}\,. \tag{1}$$

FSD is the fractional standard deviation and T is the run time in minutes. FOM indicates a tally is reliable if it is approximately constant. Maximizing FOM by applying variance reduction schemes optimizes the Monte Carlo calculation, and as such it is a measure of calculation efficiency. For a desired FSD the required run time is inversely proportional to FOM. For our comparisons we use none of the variance reduction methods offered in MCNPX so that we are considering only the effect of multigroup versus continuous energy calculation mode. We expect the various variance reduction techniques to require tailoring for the calculation mode. An optimal method in one mode may not be optimal in the other.

Fully forward transport calculations can be performed with MCNPX using either multigroup or continuous energy data. Adjoint calculations can only be run using multigroup data. A fully adjoint calculation is not an appropriate approach for beams since the response function would be a delta function in angle. However, midway forward-adjoint coupling methods that have been demonstrated as being efficient for neutron and photon transport [7,8,9], could also be efficient for coupled proton-neutron transport problems. The cited neutral particle works used a modified version of the MCNP code that couples forward and adjoint flux solutions for given energy, surface, polar angle and azimuthal angle discretizations on a midway surface to calculate a desired detector response [10]. We are alternatively using the surface source feature in MCNPX without modification of the code and use spherical harmonics rather than angular binning in the coupling.

2. OUT-OF-BEAM ADJOINT METHOD

MCNPX includes an option to write surface source files during transport calculations. When a particle crosses specified surfaces, type, weight, energy, time, position and direction information is recorded in these files. Normally, subsequent transport calculations are run starting these particles from the surface. In our out-of-beam adjoint method we run a forward simulation of the beam incident on a model writing a surface source file with tracks leaving a cylinder about the beam and adjoint simulations writing surface source files with tracks entering the cylinder. Coupling forward and adjoint angular flux solutions obtained from the surface source files permits detector responses to be calculated. The efficiency of this method is realized in studies involving variations of the in-beam portion of the problem. A single set of adjoint calculations for the desired detector responses is required. And since the forward simulations need only consider the in-beam transport, subsequant solutions can be obtained more efficiently than running the full forward calculation.

Adjoint calculations can only be run with MCNPX using multigroup cross section data. Forward calculations can be run using either multigroup or continuous energy cross section data. We can couple adjoint out-of-beam simulations with both multigroup and continuous energy in-beam simulations. In the surface source files written by multigroup calculations the group number is provided as the particle energy. The particle type is the same for protons and neutrons in this case since the protons are masqueraded as neutrons in the library and transport calculation. In the continuous energy case the actual energy and particle type are provided.

The position of a particle crossing in the surface source file is given as an (x,y,z) point in the coordinate system of the model. The direction is given in terms of u, v, the sign of w, and μ, where u, v and w are projections of the unit direction vector onto axes parallel to the x, y and z axes respectively and μ is the cosine of the angle between the direction vector $\hat{\Omega}$ and the surface normal $\hat{n}$ at the crossing point. Fig. 1 is a sketch depicting a model where the surface bounding the in-beam problem is a cylinder on the z-axis. The out-of-beam problem has a spherical detector volume in another cylinder whose axis is parallel to the x-axis. We used this model to study our out-of beam adjoint method with detector volumes at various distances from the in-beam bounding surface. We filled the cylinder parallel to the x-axis with water and placed an annular aluminum collimator in the portion of the in-beam cylinder above the water cylinder. Proton beams were modeled about the z-axis in the negative direction. This is a simple model approximating problems where stray radiation doses from proton therapy beams are calculated.

From Ref. 11 the general equation for the detector response in terms of the adjoint flux solution ψ^+ and a known distribution of incoming particles $\tilde{\Psi}$ on an adjoint problem boundary surface Γ is

$$R = \int d\Gamma \int dE \int_{\hat{n}\cdot\hat{\Omega}<0} d\Omega \left|\hat{n}\cdot\hat{\Omega}\right| \psi^+ \tilde{\Psi} \,. \tag{2}$$

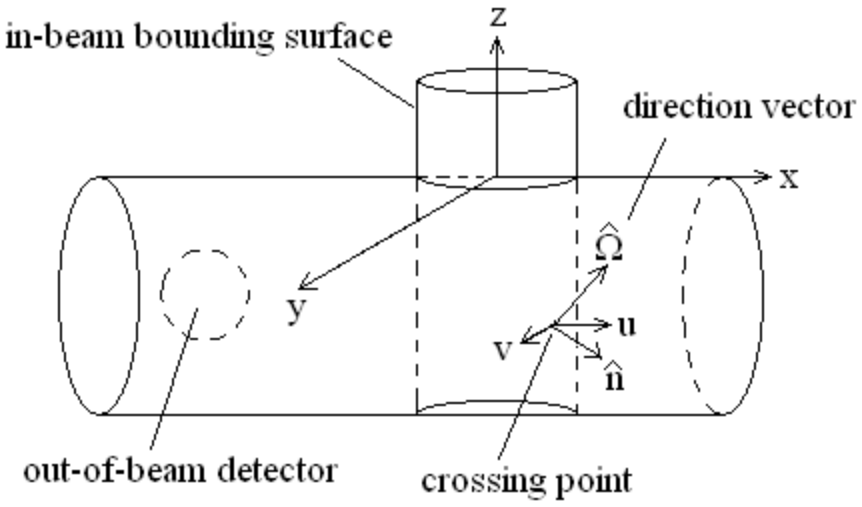

Figure 1. Sketch of model used for out-of-beam adjoint method studies.

The forward in-beam transport calculation provides $\tilde{\Psi}$. To solve Eq. 2 we segment the bounding surface with planes perpendicular to the z-axis. This forces an axial symmetry assumption for the in-beam geometry. Circumferential segmentation as well would relax this. We use the multigroup cross section library's energy discretization. For particles crossing the bounding surface we compute 4π-normalized real spherical harmonic coefficients by energy group and segment of the function $d\Gamma dE\left|\hat{n}\cdot\hat{\Omega}\right|\psi^{+}$ for adjoint particles and $\tilde{\Psi}$ for forward particles. Identifying these coefficients as $A_{i,g,l,m}$ for the adjoint function and $F_{i,g,l,m}$ for the forward function permits Eq. 2 to be estimated numerically using

$$R\approx\sum_{i=1}^{I}\sum_{g=1}^{G}\sum_{l=0}^{L}\sum_{m=-l}^{l}A_{i,g,l,m}F_{i,g,l,m}\,, \tag{3}$$

where I is the number of surface segments, G is the number of energy groups, and L is the degree at which the spherical harmonics expansion is truncated. The coefficients are calculated by summing over the crossings in the respective adjoint and forward surface source files using

$$A_{i,g,l,m}=\sum_{c=1}^{C_A}\begin{cases}\dfrac{w_c}{N_A}Y_{l,m}\left(-\mu_c,\pi+\phi_c\right), \text{ if crossing } c \text{ in segment } i \text{ and group } g\\ 0, \text{ otherwise}\end{cases}, \text{ and} \tag{4}$$

$$F_{i,g,l,m}=\sum_{c=1}^{C_F}\begin{cases}\dfrac{w_c}{N_F\mu_c\Delta\Gamma_i\Delta E_g}Y_{l,m}\left(\mu_c,\phi_c\right), \text{ if crossing } c \text{ in segment } i \text{ and group } g\\ 0, \text{ otherwise}\end{cases}. \tag{5}$$

In Eqs. 4 and 5 w_c is the weight of the particle crossing the surface, C_A and C_F are the total number of particle crossings in the respective surface source files, N_A and N_F are the number of source particle histories sampled for creation of the respective surface source files, $\Delta\Gamma_i$ is the surface area of the segment crossed, and ΔE_g is the width of the energy group in which the crossing particle's energy lies. μ_c is the cosine of the angle between the crossing particle direction vector $\hat{\Omega}$ and the outward directed surface normal $\hat{n}$. ϕ_c is the azimuthal angle measured from the radial tangent. Since the adjoint particle crossings are providing the detector response for forward particles traveling in the opposite direction, the sign of adjoint μ_c is changed and 180º is added to adjoint ϕ_c. μ_c are provided explicitly in the surface source files. ϕ_c are computed by geometric transformation from the MCNPX spatially aligned coordinate system. The $Y_{l,m}(\mu_c,\phi_c)$ are real normalized spherical harmonics functions defined as

$$Y_{l,m}(\mu_c,\phi_c)=\begin{cases}\overline{P}_{l,m}(\mu_c)\cos m\phi_c, \text{ if } m\geq 0\\ \overline{P}_{l,|m|}(\mu_c)\sin|m|\phi_c, \text{ if } m<0\end{cases} \tag{6}$$

where the normalization of the associated Legendre functions $P_{l,m}(\mu_c)$ is given by

$$\overline{P}_{l,m}(\mu_c)=\sqrt{(2-\delta_{0,m})(2l+1)\frac{(l-m)!}{(l+m)!}}P_{l,m}(\mu_c). \tag{7}$$

Our spherical harmonic analyses were performed using the freely available software archive SHTOOLS (available at http://www.ipgp.fr/~wieczor/SHTOOLS/SHTOOLS.html). Specifically the PlmBar routine of SHTOOLS computes Eq. 7.

Sums of squares of the contributions to the spherical harmonic coefficients $A_{i,g,l,m}$ and $F_{i,g,l,m}$ are calculated for estimation of the standard deviation of detector response given by Eq. 3 in accordance with the central-limit theorem. Since the coefficients are statistically independent the sum of their relative variances approximates the relative variance of their products [7]. Using $r^2(x)$ to denote relative variance of x this is expressed as

$$r^2\left(A_{i,g,l,m}F_{i,g,l,m}\right)=r^2\left(A_{i,g,l,m}\right)+r^2\left(F_{i,g,l,m}\right). \tag{8}$$

With the variables as defined for Eqs. 4 and 5 the relative variances of $A_{i,g,l,m}$ and $F_{i,g,l,m}$ are respectively

$$r^2\left(A_{i,g,l,m}\right)=\frac{1}{A_{i,g,l,m}^2}\sum_{c=1}^{C_A}\begin{cases}\left[\frac{w_c}{N_A}Y_{l,m}(-\mu_c,\pi+\phi_c)\right]^2, c \text{ in } i \text{ and } g\\ 0, \text{ otherwise}\end{cases}-\frac{1}{N_A}, \text{ and} \tag{9}$$

$$r^2\left(F_{i,g,l,m}\right)=\frac{1}{F_{i,g,l,m}^2}\sum_{c=1}^{C_F}\left\{\begin{array}{l}\left[\dfrac{w_c}{N_F\mu_c\Delta\Gamma_i\Delta E_g}Y_{l,m}\left(\mu_c,\phi_c\right)\right]^2,\ c \text{ in } i \text{ and } g\\ 0, \text{ otherwise}\end{array}\right\}-\frac{1}{N_F}. \tag{10}$$

The variance of the Eq. 3 detector response is then given by the sum of the absolute variances,

$$\sigma^2=\sum_{i=1}^{N}\sum_{g=1}^{G}\sum_{l=0}^{L}\sum_{m=-l}^{l}r^2\left(A_{i,g,l,m}F_{i,g,l,m}\right)A_{i,g,l,m}^2F_{i,g,l,m}^2\ . \tag{11}$$

The FSD used in calculating FOM is then

$$\text{FSD}=\frac{\sigma}{R}. \tag{12}$$

We stated that we only write outward tracks crossing the boundary cylinder for the forward part of the problem and inward tracks for the adjoint part. However, particles scattering back and forth across the boundary must also be accounted for. This is accomplished using the black absorber technique proved in Ref. 7. One of the problems, in-beam forward or out-of-beam adjoint, must track particles in both directions and the other must see its counterpart as fully absorbing. We run the adjoint simulations with the in-beam portion of the model as a black absorber using zero importance. Therefore the forward in-beam simulation must include some amount of important out-of-beam material.

In order for Eq. 3 to give a meaningful detector response the forward in-beam and adjoint out-of-beam sources must be specified appropriately. For the forward simulation actual beam parameters are defined. From the Ref. 11 definition of the adjoint problem, the adjoint source is isotropic, uniformly sampled over the detector volume, with a group-wise energy probability density function given by

$$P_g=\frac{\Delta E_g\Sigma_g}{\sum_{g=1}^{G}\Delta E_g\Sigma_g}, \tag{13}$$

where Σ_g is a cross section for the detector response. We have used the energy deposition cross sections from the multigroup library. Provided an adjoint source particle weight of $\sum_{g=1}^{G}\Delta E_g\Sigma_g$ and a forward source particle weight of one, Eq. 3 provides total response in energy deposited per unit volume per incident forward source particle. To compute energy deposition from neutrons and protons separately, two adjoint out-of beam calculations are run. Rather than indexing from $g=1$ to G in Eq. 13 and in the weight computation, the range is over relevant proton and neutron groups separately. Regardless, only one forward in-beam simulation is

required. The two adjoint simulations provide separate neutron and proton detector responses to the forward particles, both proton and neutron, leaving the in-beam problem.

3. TEST PROBLEM DEFINITION

Fig. 2 is plot of our test problem model geometry. We assume a 157.5 MeV proton beam, midrange for therapy beam energies, is incident on a stopping length (10 cm) aluminum collimator abutted to the side of a water cylinder 100 cm long and 30 cm in diameter. The geometry is intended to be a simplified approximation of a proton therapy application where the water simulates a phantom or patient and the collimator simulates beam line components where secondary neutrons are produced outside the body. The range of the beam protons in water is 17 cm. The outside diameter of the beam and collimator is 4 cm. The inside diameter of the collimator is 0.6 cm. Spatially the beam is assumed to have a Gaussian distribution with a 0.6 cm full width at half maximum (FWHM) in both x and y. This puts half of the beam through the collimator and half incident on its annulus.

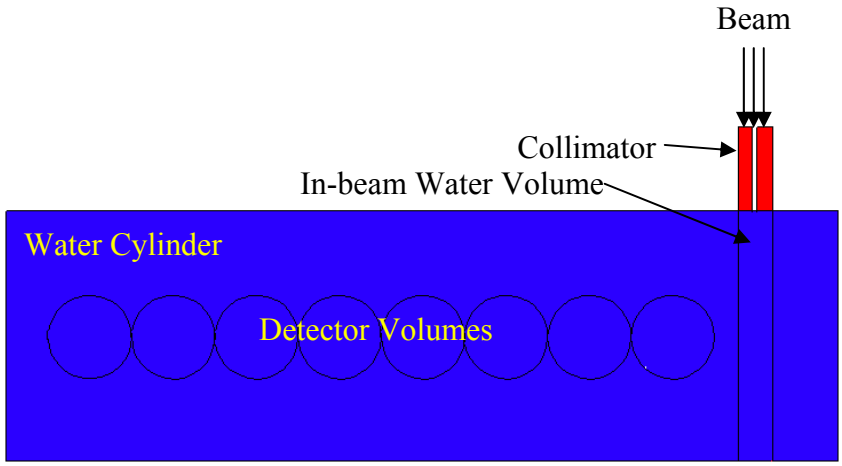

Figure 2. MCNPX plot of test problem geometry.

The beam axis is normal to the side of the water cylinder and is 10 cm from one end. Detector volumes 10 cm in diameter are included along the axis of the water cylinder at 10 cm intervals. These are intended to simulate organs for which doses are calculated. The water column beneath the collimator is specified as a cell defining in-beam water volume. The in-beam bounding surface for which surface source files are written extends from the top of the collimator to the bottom of the water cylinder.

4. RESULTS

We first solve the test problem with fully forward transport using both continuous energy and multigroup cross section data to compare results and calculation efficiencies. What we are

calculating is average energy deposition from neutrons and protons in the detector volumes of Fig. 2. We then solve the problem using our out-of-beam adjoint method. Again we compare results and calculation efficiencies but begin by evaluating sensitivity to the truncation degree of the spherical harmonic expansions, refinement of surface segmentation, and the amount of out-of-beam material included in the forward simulation.

4.1. Fully Forward Calculations

Fig. 3 compares forward MCNPX multigroup and continuous energy transport solutions after 50 million histories. For the continuous energy calculations we are using type f6 energy deposition tallies. For the multigroup calculations we are using type f4 flux tallies multiplied by the energy deposition cross sections of the multigroup library. The agreement is good and generally within calculation uncertainty for both the neutron and proton energy deposition solutions. Table I compares the FOM of the multigroup and continuous energy calculations. The FSDs for the multigroup and continuous energy tallies are comparable. This implies that FOM ratios are required run time ratios for desired FSD. For this calculation multigroup transport is about 30 times faster than continuous energy.

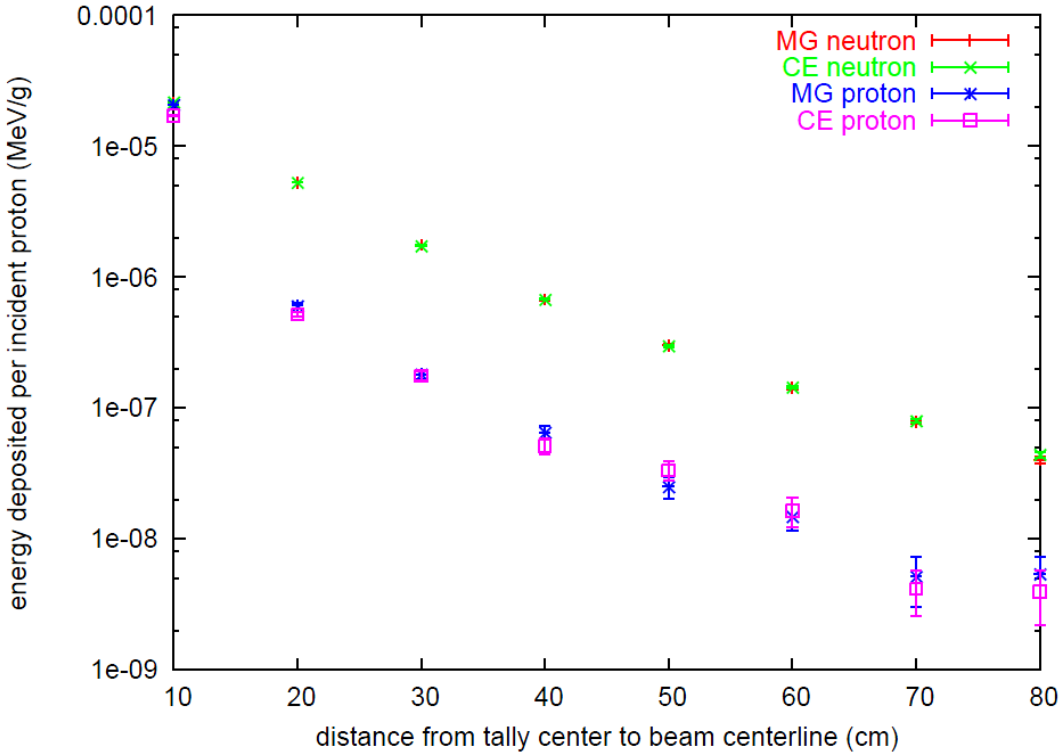

Figure 3. Energy deposition tally results for fully forward multigroup (MG) and continuous energy CE calculations.

Table I. Multigroup (MG) to continuous energy (CE) FOM ratios.

Tally Center to Beam Axis (cm)	FOM Ratios (MG:CE)	
	Neutron	Proton
10	27	34
20	27	29
30	27	27
40	26	34
50	27	23
60	27	37
70	26	23
80	25	47

4.2. Out-of-Beam Adjoint Calculations

Out-of-beam adjoint transport was run for the eight detector volumes sampling adjoint source particles from energy probability density functions defined by the neutron and proton energy deposition cross sections separately. The in-beam cells of the Fig. 2 model were given an importance of zero for the black absorber technique. Surface source files were written for each of the sixteen detector-particle type combinations recording tracks crossing the in-beam bounding surface with negative sense. It was found that some form of variance reduction is necessary for practical adjoint simulation efficiency. From the full forward calculations it was observed that essentially all of the energy deposition occurs within 10 shakes. Noting this we terminated adjoint histories after 10 shakes. We also biased the sampling of the energy probability density function such that all groups were sampled uniformly. The Eq. 4 coefficients and Eq. 10 relative variances were calculated from the adjoint surface source file data assuming 1, 2, 4, 8, 16, 20, 40, 60, 80 and 100 surface segments and spherical harmonic expansion truncation degrees from $L = 0$ to 40.

The forward in-beam transport was run analog in both multigroup and continuous energy modes with 0, 2, 4, 6 and 8 cm of out-of-beam material included radially. Surface source files were written for these ten cases and the Eq. 5 coefficients and Eq. 11 relative variances were calculated for the same segmentation and truncation degree assumptions as for the adjoint calculations. The detector responses and response variances were then calculated according to Eqs. 3 and 12 respectively, for various combinations of surface segmentation, truncation degree and included scattering material thickness assumptions.

Varying the amount of out-of-beam material included in the forward in-beam transport simulation did not have an observable effect on the detector responses. This implies that the contribution from particles leaving the in-beam portion of the problem, scattering back in, then

leaving again or creating more particles that leave is insignificant for the test problem. Higher spherical harmonic truncation degrees are required for more distant detectors. Fig. 4 illustrates this. It is a plot of neutron energy deposition solutions obtained truncating spherical harmonic expansions at 0 to 40 degrees, using multigroup forward in-beam transport. $L = 40$ appears sufficient for neutron detectors at distances up to about 80 cm. For proton detectors higher degree expansions appear necessary for accurate solutions as illustrated in Fig. 5. Proton errors are large for the four most distant detectors. The protons that are depositing energy in nearest detector include secondary particles produced in beam proton interactions. For the more distant detectors the protons are tertiary, being created by high energy secondary neutrons from beam interactions. From a total energy deposition perspective, that from tertiary protons in the distant detectors is an order of magnitude less than that directly deposited by neutron interactions. Regarding surface segmentation, it appears as may be expected that segment length should to be small compared to detector size. Neutron and proton energy deposition solutions as a function of number of uniformly sized segments are presented in Figs. 6 and 7. With 16 or more segments the results are statistically indistinguishable.

Table II lists the fully forward calculation results plotted in Fig. 3 along with the out-of-beam adjoint results for the 16-segment, no albedo material solutions. Fractional differences comparing out-of-beam adjoint results to fully forward results are calculated. The neutron out-of-beam adjoint results are generally within 10 percent of the full forward results. Differences are systematically highest at even distances in decimeters (20, 40, 60 and 80 cm), appearing to be a harmonic interference pattern, suggesting an instability in our method requiring further investigation. Differences are somewhat smaller for continuous energy forward results than they are for the multigroup forward results. Agreement is remarkably good comparing the multigroup proton results. For detectors nearer the beam where calculation errors are acceptable, differences are within calculation uncertainty. Since the multigroup calculations use the same cross section data for full forward, out-of-beam adjoint and in-beam forward transport, any differences should be attributable to systematic errors introduced by our out-of-beam adjoint method. We have not yet determined a reason for the out-of-beam adjoint proton energy deposition solutions appearing better than the neutron solutions.

The adjoint transport and adjoint coefficient calculations are relatively time consuming. However, they only have to be performed once for each detector and then any number of in-beam simulations can be run with detector responses readily calculated using the coupling coefficients. Table III lists FOM ratios where the out-of-beam adjoint FOMs are calculated using total time. Total time is the sum of adjoint transport, adjoint coefficient calculation, coupling calculation, forward in-beam transport, and forward coefficient calculation times. For a single calculation the out-of-beam adjoint method is generally not as efficient as fully forward continuous energy transport. If several in-beam perturbations are to be made, the out-of-beam adjoint method could be more efficient. Table IV lists FOM ratios where the out-of-beam adjoint FOMs are calculated using the sum of coupling calculation, forward in-beam transport, and forward coefficient calculation times. There is no benefit for running continuous energy in-beam transport coupled with out-of-beam adjoint for the detectors nearer than about 30 cm. Efficiency gains for secondary neutron dose calculations increase with distance to the detector. For our most distant detector running continuous energy in-beam with adjoint coupling is about 10 times faster than full forward continuous energy and running multigroup in-beam is about 50 times faster.

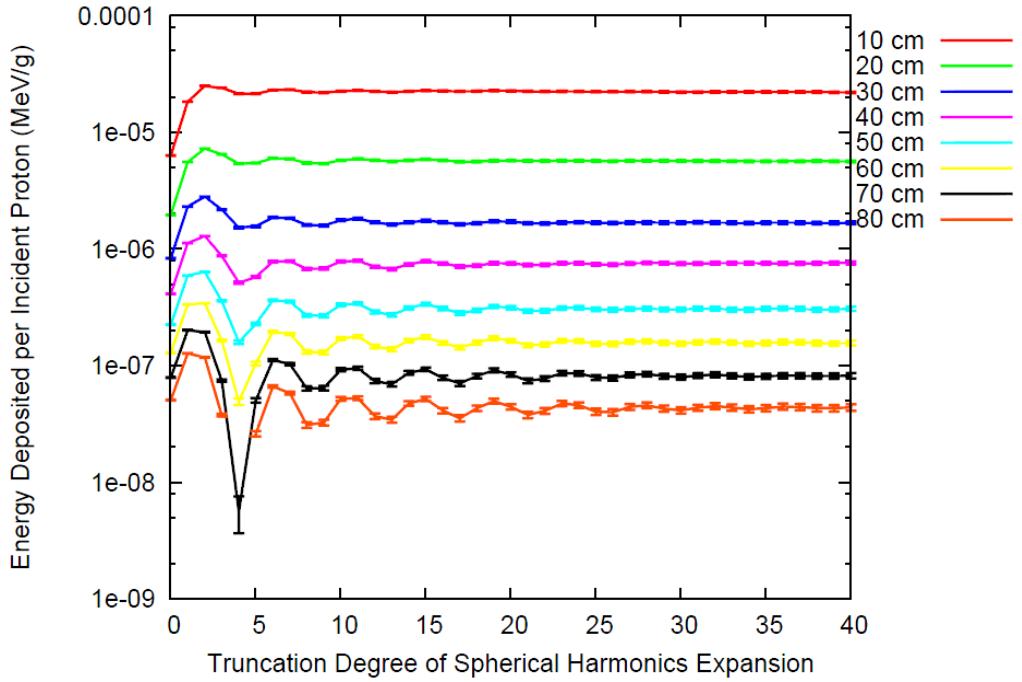

Figure 4. Neutron energy deposition results for out-of-beam adjoint method as a function of spherical harmonics truncation degree.

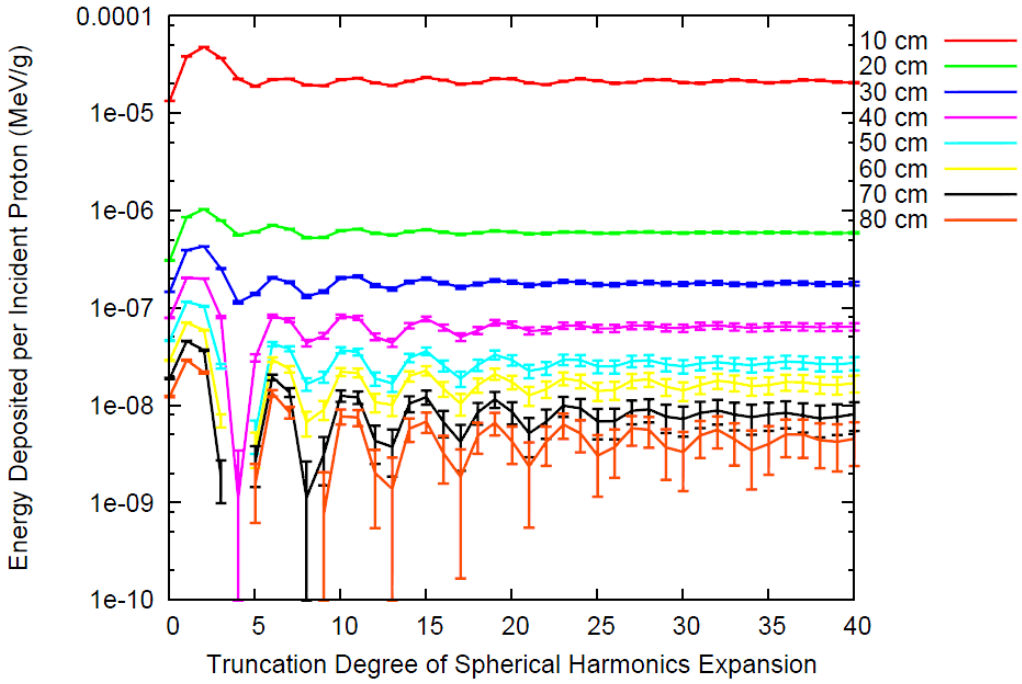

Figure 5. Proton energy deposition results for out-of-beam adjoint method as a function of spherical harmonics truncation degree.

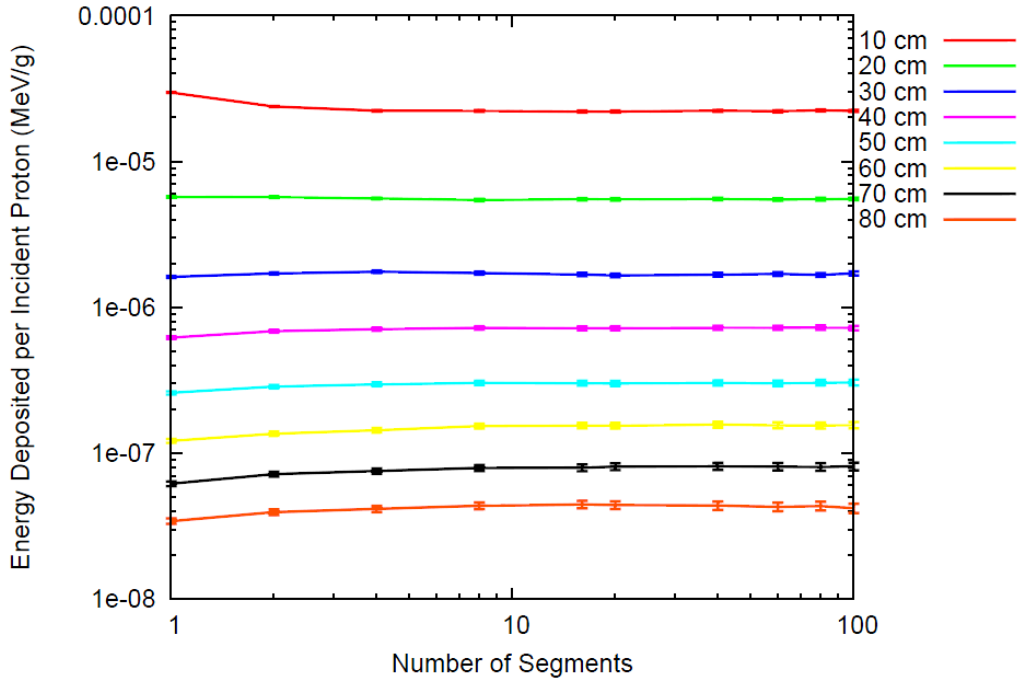

Figure 6. Neutron energy deposition results for out-of-beam adjoint method as a function of the number of boundary surface segments.

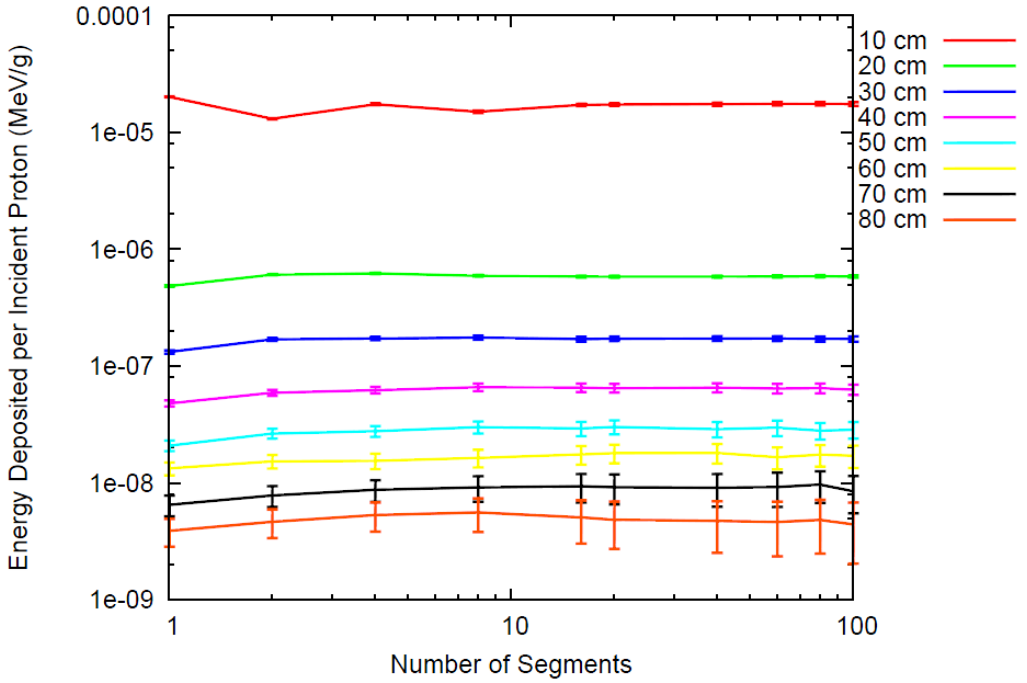

Figure 7. Proton energy deposition results for out-of-beam adjoint method as a function of the number of boundary surface segments.

Table II. Energy deposition calculation results.

Tally Center to Beam Axis (cm)	Fully Forward (MeV/g)	Fully Forward FSD	Out-of-Beam Adjoint (MeV/g)	Out-of-Beam Adjoint FSD	Fractional Difference
MG Full Forward and MG In-Beam Neutron Results					
10	2.14E-05	0.002	2.22E-05	0.015	0.038
20	5.26E-06	0.005	5.67E-06	0.020	0.078
30	1.75E-06	0.008	1.72E-06	0.027	-0.020
40	6.70E-07	0.013	7.52E-07	0.031	0.122
50	3.00E-07	0.020	3.09E-07	0.040	0.031
60	1.43E-07	0.028	1.58E-07	0.045	0.106
70	7.83E-08	0.039	8.10E-08	0.054	0.035
80	4.00E-08	0.054	4.45E-08	0.062	0.112
CE Full Forward and CE In-Beam Neutron Results					
10	2.17E-05	0.002	2.21E-05	0.015	0.020
20	5.27E-06	0.005	5.54E-06	0.020	0.051
30	1.73E-06	0.008	1.69E-06	0.027	-0.023
40	6.74E-07	0.013	7.23E-07	0.030	0.073
50	2.98E-07	0.019	3.04E-07	0.039	0.022
60	1.44E-07	0.027	1.55E-07	0.044	0.077
70	7.99E-08	0.037	8.03E-08	0.053	0.004
80	4.41E-08	0.050	4.49E-08	0.059	0.019
MG Full Forward and MG In-Beam Proton Results					
10	2.07E-05	0.009	2.10E-05	0.016	0.015
20	6.02E-07	0.044	6.01E-07	0.020	-0.001
30	1.81E-07	0.077	1.79E-07	0.044	-0.008
40	6.50E-08	0.125	6.48E-08	0.088	-0.003
50	2.50E-08	0.189	2.72E-08	0.154	0.088
60	1.48E-08	0.226	1.68E-08	0.197	0.133
70	5.17E-09	0.417	8.12E-09	0.325	0.570
80	5.39E-09	0.345	4.83E-09	0.439	-0.104
CE Full Forward and CE In-Beam Proton Results					
10	1.71E-05	0.010	1.74E-05	0.024	0.014
20	5.19E-07	0.044	5.90E-07	0.020	0.137
30	1.76E-07	0.074	1.72E-07	0.045	-0.024
40	5.11E-08	0.136	6.58E-08	0.083	0.289
50	3.35E-08	0.172	2.93E-08	0.140	-0.124
60	1.64E-08	0.257	1.77E-08	0.182	0.081
70	4.14E-09	0.377	9.46E-09	0.275	1.284
80	3.95E-09	0.445	5.16E-09	0.401	0.306

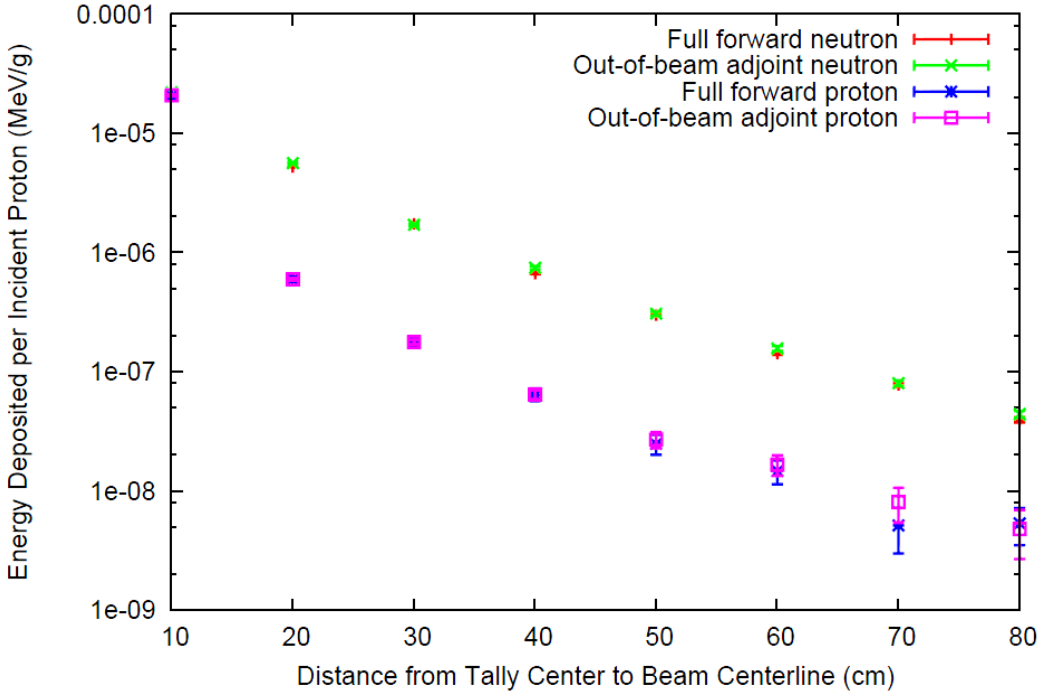

Figure 8. Energy deposition results for fully forward multigroup transport and out-of-beam adjoint method with multigroup in-beam transport.

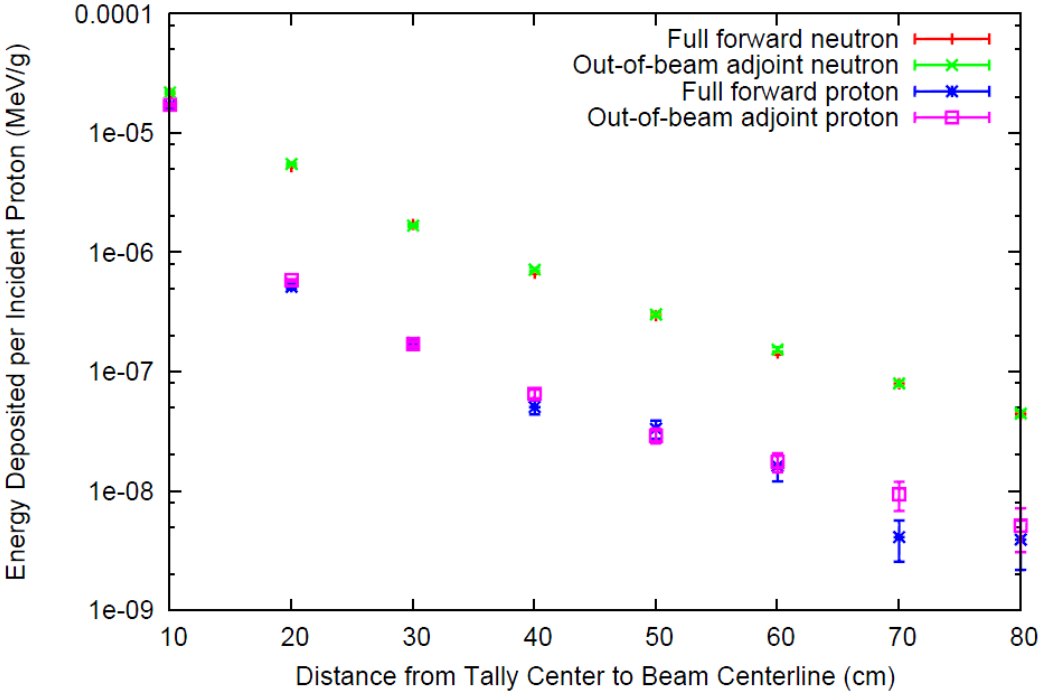

Figure 9. Energy deposition results for fully forward continuous energy transport and out-of-beam adjoint method with continuous energy in-beam transport.

Table III. Out-of-beam adjoint to fully forward continuous energy FOM ratios calculated using total time.

Tally Center to Beam Axis (cm)	FOM Ratios (out-of-beam adjoint:fully forward CE)			
	Neutron		Proton	
	MG in-beam	CE in-beam	MG in-beam	CE in-beam
10	0.32	0.15	0.37	0.15
20	0.38	0.25	1.52	1.52
30	0.29	0.24	0.90	0.87
40	0.30	0.27	0.78	0.84
50	0.22	0.22	0.40	0.47
60	0.20	0.21	0.53	0.60
70	0.16	0.16	0.42	0.57
80	0.15	0.17	0.32	0.37

Table IV. Out-of-beam adjoint to fully forward continuous energy FOM ratios calculated using sum of coupling calculation, forward in-beam transport, and forward coefficient calculation times.

Tally Center to Beam Axis (cm)	FOM Ratios (out-of-beam adjoint:fully forward CE)			
	Neutron		Proton	
	MG in-beam	CE in-beam	MG in-beam	CE in-beam
10	1.8	0.2	28	1.8
20	4.3	0.6	376	55
30	6.7	1.0	223	32
40	14	2.0	193	31
50	18	2.8	99	17
60	29	4.4	137	23
70	37	5.5	108	22
80	52	8.3	82	14

We compiled MCNPX, the SHTOOLS library and our forward-adjoint coupling code with the free gfortran compiler. We ran our calculations on a Linux platform with two quad core 2.5 GHz processors, 16 GB of RAM and 160 GB of hard disk. This modest configuration was suitable for the high order spherical harmonic expansions needed, suggesting our out-of-beam adjoint method is computationally practical.

Though we still must resolve the discrepancies between out-of-beam adjoint and fully forward transport results, the agreement we have observed and the potential for efficiency gains are encouraging. We averaged energy deposition over relatively large detector volumes. For smaller detectors, the ratios of out-of-beam adjoint to fully forward FOMs are expected to be higher since smaller detector size will decrease the fully forward FOM while smaller adjoint source volume should have little effect on the out-of-beam adjoint FOM. We plan to perform the forward-adjoint midway coupling using angle binning to isolate any systematic errors introduced by our spherical harmonics approach. One motivation for using spherical harmonics coupling is that it lends itself to using deterministic transport methods for the out-of-beam transport, forward or adjoint. We also plan to evaluate efficiency improvements that may be achievable with deterministic out-of-beam transport.

5. CONCLUSIONS

We have showed that coupled proton/neutron multigroup transport can be 30 times more efficient than continuous energy transport using MCNPX for calculating secondary neutron doses from proton therapy beams. This is for fully forward simulations and agreement between multigroup and continuous energy is generally within Monte Carlo calculation error. We also presented a variation of the midway forward-adjoint coupling method where we use the MCNPX surface source capability and spherical harmonic expansions for coupling in angle. Using our out-of-beam adjoint method we obtain secondary neutron dose results that are generally within 10 percent of fully forward transport results. We expect better agreement to be achievable and continue to investigate. The out-of-beam adjoint method is not more efficient than fully forward transport unless the adjoint coefficients are going to be used to determine detector responses for a number of forward in-beam simulations, in which case the method can be an order of magnitude more efficient for distant detectors.

REFERENCES

1. D. J. Brenner and E. J. Hall, “Secondary neutrons in clinical proton radiotherapy: A charged issue,” *Radiotherapy and Oncology*, **86**, pp. 165-170 (2008).
2. W. Newhauser, N. Koch and U. Titt, “Prediction of Absorbed Dose Distributions and Neutron Dose Equivalent Values in Proton Beam Radiation Therapy,” ANS-RT-PROTON-01, Computational Medical Physics Working Group, American Nuclear Society (2007).
3. D. B. Pelowitz (ed.), “MCNPX User’s Manual,” LA-CP-07-1473, Version 2.6.0, Los Alamos National Laboratory (2008).
4. Y. Zheng, W. Newhauser, J. Fontenot, N. Koch and R. Mohan, “Monte Carlo simulations of stray neutron radiation exposures in proton therapy,” *Journal of Nuclear Materials*, **361**, pp. 289-297 (2007).
5. C. T. Kelsey IV and A. K. Prinja, “Multigroup Neutron Dose Calculations for Proton Therapy,” *International Conference on Mathematics, Computational Methods & Reactor Physics (M&C 2009)*, Saratoga Springs, New York, May 3-7, 2009, on CD-ROM, American Nuclear Society, LaGrange Park, IL (2009).
6. C. T. Kelsey IV and A. K. Prinja, “Coupled Multigroup Proton/Neutron Cross Sections for Deterministic Transport,” *Nuclear Technology*, **168**, pp. 257-263 (2009).

7. I. V. Serov, T. M. John and J. E. Hoogenboom, "A Midway Forward-Adjoint Coupling Method for Neutron and Photon Monte Carlo Transport," *Nuclear Science and Engineering*, **133**, pp. 55-72 (1999).
8. T. Ueki and J. E. Hoogenboom, "Exact Monte Carlo Perturbation Analysis by Forward-Adjoint Coupling in Radiation Transport Calculations," *Journal of Computational Physics* **171**, pp. 509-533 (2001).
9. T. Ueki, J. E. Hoogenboom and J. L. Kloosterman, "Analysis of Correlated Coupling of Monte Carlo Forward and Adjoint Histories," *Nuclear Science and Engineering*, **137**, pp. 117-145 (2001).
10. J. F. Briesmeister (ed.), "MCNP – A General Monte Carlo N-Particle Transport Code," LA-12625-M, Version 4B, Los Alamos National Laboratory (1997).
11. E. Lewis, W. Miller, *Computational Methods of Neutron Transport*, pp. 47-52, American Nuclear Society, La Grange Park, Illinois (1993).